

New determinations of the critical velocities of C-type shock waves in dense molecular clouds: application to the outflow source in Orion

J. Le Bourlot,¹ G. Pineau des Forêts,² D. R. Flower³★ and S. Cabrit⁴

¹DAEC, Observatoire de Paris, F-92195 Meudon Principal Cedex, France

²IAS, Université de Paris-Sud, F-92405 Orsay, France

³Physics Department, The University, Durham DH1 3LE

⁴DEMIRM, Observatoire de Paris, UMR 8540 du CNRS, 61 Avenue de l'Observatoire, F-75014 Paris, France

Accepted 2002 January 29. Received 2002 January 29; in original form 2001 October 23

ABSTRACT

We report calculations of the intensities of rovibrational transitions of H₂ emitted from C-type shock waves propagating in molecular gas. Attention was paid to the thermal balance of the gas and to the rates of collisional dissociation and ionization of H₂. We found that the maximum shock speeds which can be attained, prior to the collisional dissociation of H₂ (which results in a sonic point in the flow and hence a J-type shock wave), can be much higher than had previously been believed. Thus, adopting the ‘standard’ scaling of the transverse magnetic induction with the gas density, $B(\mu\text{G}) = [n_{\text{H}}(\text{cm}^{-3})]^{1/2}$, we established that the maximum shock speed increased from 20–30 km s⁻¹ at high pre-shock densities ($n_{\text{H}} \geq 10^6 \text{ cm}^{-3}$) to 70–80 km s⁻¹ at low densities ($n_{\text{H}} \leq 10^4 \text{ cm}^{-3}$). The critical shock speed, v_{crit} , also increases significantly with the transverse magnetic induction, B , at a given pre-shock gas density, n_{H} . By way of an application of these results, we demonstrate that a two-component model, comprising shock waves with velocities $v_s = 60$ and 40 km s⁻¹, reproduces the column densities of H₂ observed by ISO-SWS up to the highest level (possibly) detected, $v = 0, J = 27$, which lies 42 515 K above the ground state. We found no necessity to invoke mechanisms other than thermal collisional excitation in the gas phase; but the $v = 1$ vibrational band remains less completely thermalized than is indicated by the observations. Fine structure transitions of atoms and ions were also considered. The intensity of the [Si I] 68.5 μm transition, observed by Gry et al. using ISO-LWS, is satisfactorily reproduced by the same model and may also originate in OMC-1, rather than Orion-KL as originally believed. The transitions of [Fe II] and [S I] observed by Rosenthal et al. may also arise in the shock-heated gas.

Key words: molecular processes – shock waves – ISM: individual: Orion OMC-1 – ISM: molecules.

1 INTRODUCTION

The properties of continuous (C-type) shock waves, propagating in dense molecular clouds of the interstellar medium, have been investigated by Draine, Roberge & Dalgarno (1983), Pineau des Forêts, Flower & Dalgarno (1988), Smith & Brand (1990), Kaufman & Neufeld (1996a,b), Timmermann (1998) and recently by Wilgenbus et al. (2000). Such studies contribute to our understanding of molecular outflows observed in regions of star formation. By means of the models, predictions have been made of the intensities of atomic fine structure transitions and of rotational transitions of molecules such as CO and H₂O. In addition, the intensities of rovibrational transitions of H₂ have been calculated,

assuming various initial values of the ortho:para H₂ ratio, and compared with ISO and ground-based observations of outflow sources, notably HH54 (Timmermann 1998; Neufeld, Melnick & Harwit 1998; Wilgenbus et al. 2000).

The heating of the gas associated with the shock wave can give rise to the excitation of H₂ and to its dissociation. The greater is the speed of a shock wave, propagating into a medium with a given set of initial conditions, the higher are the maximum temperature attained and the rate of collisional dissociation of H₂. Because H₂ is the main coolant, the dissociation of H₂ is accompanied by a rapid increase in the kinetic temperature of the gas, resulting in a sonic point in the flow – i.e. the shock wave becomes jump (J) type. Ionization of H₂, H and He by streaming ions might also limit the maximum speed, v_{crit} , which is consistent with a C-type shock wave. For pre-shock gas densities in the range

★E-mail: david.flower@durham.ac.uk

$10^4 \leq n_{\text{H}} \leq 10^6 \text{ cm}^{-3}$, Draine et al. (1983) deduced critical speeds $49 \geq v_{\text{crit}} \geq 40 \text{ km s}^{-1}$. However, the dissociation/ionization of the gas and the dynamics of the fluid flow were not treated self-consistently in their calculations. As will be seen in Section 3 below, when the physico-chemical rate equations are solved in parallel with the conservation equations describing the flow, it is found that C-type shock waves can exist up to higher values of the shock speed than was previously believed. For example, when the pre-shock gas density is 10^4 cm^{-3} , the shock wave remains C-type up to a velocity $v_{\text{crit}} = 70 \text{ km s}^{-1}$.

We have taken the opportunity to extend and update the grid of C-type shock models computed by Wilgenbus et al. (2000). In Section 2, we outline the methods that we have employed and summarize the modifications that we have made to the code since the calculations of Wilgenbus et al. In Section 3, we specify the parameter ranges used to construct the grid of models, which is made available in electronic form at <http://ccp7.dur.ac.uk/>. We calculate the maximum speed compatible with the existence of a C-type shock wave, as a function of the pre-shock gas density and magnetic field strength. As an application, we model the spectrum of H_2 and the emission in optically forbidden lines of atoms and ions from the outflow source in Orion and compare with observations made by the *Infrared Space Observatory*. Section 4 contains our concluding remarks.

2 THE THEORETICAL MODEL

We specify here the salient features of the model which has been used to perform the present calculations.

2.1 Dynamics

The dynamical variables of the problem are $v_n, v_i, \rho_n, \rho_i, \rho_-, T_n, T_i, T_e, n_n, n_i$, where v denotes a flow velocity, ρ a mass density, T a kinetic temperature, and n a number density; the subscript ‘n’ specifies the neutral fluid, ‘i’ the positively charged fluid, and ‘-’ the negatively charged fluid, which comprises electrons and PAH–negative ions. The fractional abundance of the generic polycyclic aromatic hydrocarbon (PAH), $\text{C}_{54}\text{H}_{18}$, in neutral, positively and negatively charged forms, was $n_{\text{PAH}}/n_{\text{H}} = 10^{-7}$, where $n_{\text{H}} = n(\text{H}) + 2n(\text{H}_2)$. Grains were assumed to be negatively charged, and the dust:gas mass density ratio was initially 0.0085. We correct a oversight of Wilgenbus et al. (2000) and May et al. (2000) by allowing for the differential compression of the charged grains, relative to the neutral fluid, in the shock wave. We also allow for the variation of the grain radius and mass, owing to sputtering within the shock wave, using the sputtering probabilities for silicates computed by May et al. (2000). The probability of sputtering carbon from graphite grains was assumed to be the same as for sputtering silicon from silicate grains.

2.2 Chemistry

The chemical species are atoms and ions, molecules, radicals and molecular ions containing the elements H, He, C, N, O, Mg, Si, S and Fe. The initial H: H_2 abundance ratio was in chemical equilibrium, and the initial ortho:para H_2 ratio was equal to its statistical value of 3, unless otherwise stated. The grains were assumed to have a core consisting of the representative silicate MgFeSiO_4 (olivine) or graphite and, initially, a mantle comprising species which included CH_4 , NH_3 and H_2O . The abundances of the elements, in all forms, were $n_{\text{He}}/n_{\text{H}} = 0.10$, $n_{\text{C}}/n_{\text{H}} = 3.62 \times 10^{-4}$,

$n_{\text{N}}/n_{\text{H}} = 1.12 \times 10^{-4}$, $n_{\text{O}}/n_{\text{H}} = 8.53 \times 10^{-4}$, $n_{\text{Mg}}/n_{\text{H}} = 3.85 \times 10^{-5}$, $n_{\text{Si}}/n_{\text{H}} = 3.58 \times 10^{-5}$, $n_{\text{S}}/n_{\text{H}} = 1.85 \times 10^{-5}$, $n_{\text{Fe}}/n_{\text{H}} = 3.23 \times 10^{-5}$ (Anders & Grevesse 1989); these values are the same as those adopted by Wilgenbus et al. (2000).

The 124 chemical species were connected by a set of 895 chemical reactions, including ion–neutral, neutral–neutral and electron–ion recombinations in the gas phase. The grain mantles are rapidly eroded in the shock wave. At sufficiently high shock speeds, the grain cores are also eroded (cf. May et al. 2000).

2.3 Dissociation of H_2

The collisional dissociation of H_2 by atoms and ions has been discussed by Wilgenbus et al. (2000). For thermal collisions with H, the rate coefficient $[1.0 \times 10^{-10} \exp(-52000/T_n) \text{ cm}^3 \text{ s}^{-1}]$ derives from the calculations of Dove & Mandy (1986). We have adapted this expression to allow for the excitation energy $E(v, J)$ of the initial rovibrational level (v, J) , and the rate coefficient

$$\frac{1.0 \times 10^{-10}}{n(\text{H}_2)} \sum_{v,J} n(v, J) \exp\{-[56644 - E(v, J)]/T_n\} \text{ cm}^3 \text{ s}^{-1}$$

was adopted, in which $n(v, J)$ is the level population density and $n(\text{H}_2) = \sum_{v,J} n(v, J)$; $E(v = 4, J = 29) = 56644 \text{ K}$ is the energy of the highest bound level of H_2 , relative to the $v = 0, J = 0$ ground state (Dabrowski 1984). The rate coefficient for the collisional dissociation of H_2 by H_2 was taken to be eight times smaller than for dissociation by H (Jacobs, Giedt & Cohen 1967), and the rate coefficient for dissociation by He was estimated to be a factor of 10 smaller than for dissociation by H. Electron collisional dissociation was similarly taken into account, following Flower et al. (1996, section 2.1).

2.4 Ionization of H_2 and H

Draine et al. (1983) derived formulae for the rates of collisional ionization of H_2 , H and He by streaming ions, based on estimates of the corresponding ionization cross-sections. In view of the uncertainties involved, we have assumed a constant cross-section (equation 26 of Draine et al.) for this process and a threshold energy equal to the ionization potential of H_2 (15.43 eV) or H (13.60 eV); this approach tends to overestimate the importance of the process. Ionization of He was neglected, in view of its much larger ionization potential (24.59 eV). The adopted rate coefficients were $1.1 \times 10^{-13} \exp[-179160/T_{\text{eff}}(\text{H}_2)] \text{ cm}^3 \text{ s}^{-1}$ for H_2 and $1.3 \times 10^{-13} \exp[-157890/T_{\text{eff}}(\text{H})] \text{ cm}^3 \text{ s}^{-1}$ for H. The effective temperature, T_{eff} , appearing in these expressions makes allowance for the contribution to the impact energy from ion–neutral streaming, as well as for the thermal energy of the gas. Thus, in the case of H,

$$T_{\text{eff}}(\text{H}) = \frac{m_{\text{H}} m_i (v_n - v_i)^2}{3k(m_{\text{H}} + m_i)} + \frac{(m_{\text{H}} T_i + m_i T_n)}{m_{\text{H}} + m_i},$$

where ‘i’ denotes the ion.

We took into account additionally electron collisional ionization of H and H_2 . For H, we adopted the rate coefficient $9.2 \times 10^{-10} (T_e/300)^{0.5} \exp[-157890/T_e] \text{ cm}^3 \text{ s}^{-1}$. This expression derives from Hummer (1963), who made use of experimental measurements by Fite & Brackmann (1958), which were normalized to the Born approximation at high energies. More recent measurements by Shah, Elliott & Gilberty (1987) are in good agreement with those of Fite & Brackmann (1958) up to the cross-section maximum, at a collision energy of approximately

50 eV. For H_2 , we fitted the cross-sections measured by Rapp & Englander-Golden (1965) and hence obtained a rate coefficient $1.4 \times 10^{-9} (T_e/300)^{0.5} \exp[-179\,160/T_e] \text{ cm}^3 \text{ s}^{-1}$. In the case of ionization by electrons, the contribution of streaming can be neglected, owing to the small mass of the electron.

The contributions of the above processes to the thermal balance of the neutral and charged fluids were also incorporated. In the centre of mass system, the fraction of the kinetic energy lost by A , in an endothermic binary reaction with B , is $m_B/(m_A + m_B)$. Thus, ionization of H_2 or H by streaming (predominantly heavy) ions results in kinetic energy loss mainly by the neutral fluid, whereas ionization of H_2 or H by electrons results in kinetic energy loss by the negatively charged fluid.

2.5 Level populations of H_2

The level population densities $n(v, J)$ were computed in parallel with the dynamical and chemical variables, allowing for collisional and radiative transitions between the levels and for chemical reactions that create or destroy H_2 .

Molecular hydrogen is collisionally and chemically destroyed in the shock wave but reforms, on grain surfaces, at a rate ($\text{cm}^{-3} \text{ s}^{-1}$) that is given by

$$n(H)n(\text{gr})\pi r_{\text{gr}}^2 \left[\frac{8kT_{\text{eff}}}{\pi m_H(1 + T_{\text{eff}}/30)} \right]^{0.5}$$

where

$$T_{\text{eff}} = \frac{m_H(v_n - v_i)^2}{3k} + T_n$$

and $n(\text{gr})$ and r_{gr} are the local values of the grain density (the number of grains per unit volume of gas) and the root mean square grain radius, respectively. The grains are assumed to be negatively charged and to move with the charged fluid at velocity v_i . The H_2 formation rate incorporates a probability that the H atom sticks to the grain, $1/(1 + T_{\text{eff}}/30)^{0.5}$, which tends to 1 at low temperatures ($T_{\text{eff}} \ll 30 \text{ K}$) and yields a temperature-independent formation rate at high temperatures ($T_{\text{eff}} \gg 30 \text{ K}$).

Population transfer in collisions with H , He and H_2 and with grains was taken into account, using the data of Le Bourlot, Pineau des Forêts & Flower (1999) and Pineau des Forêts et al. (2001). We note that collisions with H strongly favour vibrational, compared with pure rotational transitions. At $T_n = 1000 \text{ K}$, the rate coefficients for $v = 0 - 1$ vibrational transitions, induced by collisions with H , are typically two orders of magnitude larger than for collisions with He or H_2 (cf. Le Bourlot et al. 1999, fig. 1).

Levels (v, J) up to approximately 45 000 K above the (0, 0) ground state were included in the calculations, i.e. up to 200 levels. For $E(v, J) > 20\,000 \text{ K}$, the limit of the quantum mechanical determinations of the rate coefficients, collisions with H and with grains were taken into account, the rate coefficients being taken from the quasi-classical trajectory computations of Mandy & Martin (1993) and Pineau des Forêts et al. (2001), respectively.

2.6 Coolants

As the temperature falls towards its post-shock equilibrium value, the rate of cooling by H_2 (which includes the cooling arising from its collisional dissociation, discussed in Section 2.3) decreases and radiative cooling by species such as H_2O and CO assumes importance. The contributions of rotational transitions of H_2O , CO ,

OH and NH_3 to the cooling of the gas have been incorporated, as will be described in Section 3.2 below. We have also performed benchmark calculations in which the contributions of H_2O and CO to the cooling of the gas have been calculated following the ‘escape probability’ approach of Neufeld & Kaufman (1993); the results of these calculations are reported in Section 3.2.

The code additionally calculates the cooling owing to fine structure transitions of C^+ , C and O , using the rate coefficients for collisional excitation by H , He and H_2 specified by Le Bourlot et al. (1993) and by e^- from the sources compiled by Mendoza (1983). For Si^+ , the rate of collisional excitation by H derives from the work of Roueff (1990). The collisional rate coefficients for the excitation of the fine structure transitions of Si were assumed to be identical to those for C , as data specific to Si are not yet available. We also allowed for the $^3P - ^1D$ 630-nm transition of $[O I]$, induced by collisions with H , taking the rate coefficient for excitation ($^3P \rightarrow ^1D$) from a fit to the data of Federman & Shipsey (1983) [$5.47 \times 10^{-14} T_n^{0.245} \exp(-22\,719/T_n) \text{ cm}^3 \text{ s}^{-1}$].

2.7 Numerical solution of the differential equations

The general form of the N differential equations to be solved is

$$\frac{dy_i}{dz} = f\left(y_1, \dots, y_N, \frac{dy_1}{dz}, \dots, \frac{dy_{i-1}}{dz}, z\right), \quad (1)$$

where y_i ($i = 1, N$) are the dependent variables and z , the distance, is the independent variable. Equation (1) assumes that a steady state ($\partial y_i / \partial t = 0$) has been attained; we shall consider the issue of time-scales below. The number of coupled equations, N , is the sum of the number of dynamical variables (10), the number of chemical species (124), and the number of rovibrational levels of H_2 (up to 200).

The computer program that has been used to perform the present calculations is a completely revised version of that employed by Wilgenbus et al. (2000), updated to FORTRAN 90. The VODE algorithm (Brown, Byrne & Hindmarsh 1989) is now used to solve the coupled ordinary differential equations. A complete model of a C-type shock wave takes typically 1 minute to run on a Compaq alpha processor. The execution time is greater when the cooling by H_2O and CO is computed following the approach of Neufeld & Kaufman (1993). The calculation of the escape probability requires a knowledge of the velocity gradient, dv_n/dz . However, the equation, of the form (1) above, for the velocity gradient involves the rate of radiative cooling of the neutral fluid (cf. equation 1 of Heck, Flower & Pineau des Forêts 1990) and hence, implicitly, dv_n/dz . This circumstance leads to small step lengths being taken in the region of the shock wave in which the velocity of the neutral fluid is changing rapidly – which includes that in which H_2O and CO are significant coolants.

3 RESULTS

3.1 The grid

We have recomputed and extended the grid of C-type shock models of Wilgenbus et al. (2000). The ranges of the shock parameters are as follows:

- (i) initial densities $n_H = 10^3, 10^4, 10^5, 10^6, 10^7 \text{ cm}^{-3}$;
- (ii) initial magnetic induction $B(\mu\text{G}) = [n_H(\text{cm}^{-3})]^{1/2}$;
- (iii) shock speeds $10 \leq v_s \leq v_{\text{crit}}$, in increments not exceeding

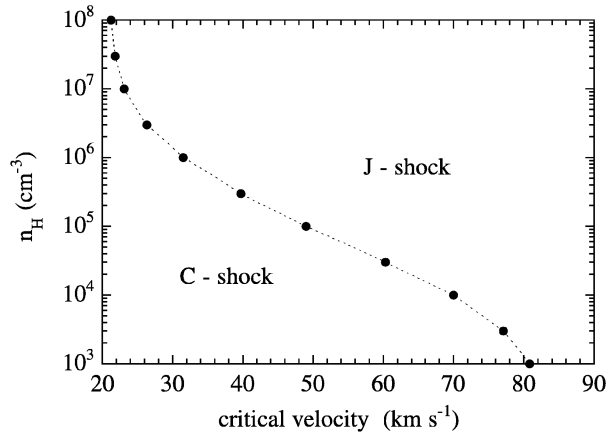


Figure 1. Maximum shock speed, v_{crit} , consistent with the existence of a C-type shock wave, as a function of the pre-shock gas density, $n_{\text{H}} = n(\text{H}) + 2n(\text{H}_2)$. The initial magnetic induction is given by $B(\mu\text{G}) = [n_{\text{H}}(\text{cm}^{-3})]^{1/2}$, and the initial ortho:para H_2 ratio is 3.0.

10 km s^{-1} , where v_{crit} depends on the initial value of n_{H} ; the maximum shock speeds are plotted in Fig. 1.

The initial ortho:para H_2 ratio was taken equal to its statistical value of 3.0. The column densities of the rovibrational levels of H_2 , obtained by integrating the population densities along the direction of shock propagation, are available in electronic form at <http://ccp7.dur.ac.uk/>.

The maximum shock speed, v_{crit} , compatible with the existence of a C-type shock wave, is plotted in Fig. 1 as a function of the pre-shock gas density, n_{H} . As may be seen from Fig. 1, the maximum shock speed that can be attained, prior to dissociation of H_2 within the shock wave (which leads to a sonic point in the flow, owing to the accompanying rapid increase in T_{n}), attains 70 km s^{-1} for a pre-shock density $n_{\text{H}} = 10^4 \text{ cm}^{-3}$ and 80 km s^{-1} for $n_{\text{H}} = 10^3 \text{ cm}^{-3}$. Thus v_{crit} exceeds the value of about 50 km s^{-1} , given originally by Draine et al. (1983) and subsequently confirmed by Smith & Brand (1990). We now consider the reasons for this apparent discrepancy.

In Fig. 2, we show the variation of the temperature T_{n} of the neutral fluid and of the fractional abundances of atomic and molecular hydrogen for models in which, initially, $n_{\text{H}} = 10^4 \text{ cm}^{-3}$, $n(\text{ortho } \text{H}_2)/n(\text{para } \text{H}_2) = 3.0$, and $v_{\text{s}} = 60$ and 70 km s^{-1} ; the ratio $n(\text{H})/n(\text{H}_2)$ initially has its equilibrium value of 7.4×10^{-4} . The temperature is plotted as a function of the flow time of the neutral fluid, derived as $t_{\text{n}} = \int (1/v_{\text{n}}) dz$. At the maximum of the temperature, the rate of collisional dissociation of H_2 is much greater than the rate of formation of H_2 on grains. In static equilibrium, the rates of formation and destruction can be equated, leading to the conclusion that $n(\text{H}) \gg n(\text{H}_2)$, i.e. that H_2 has been dissociated. However, conditions within the shock wave are not consistent with the assumption of static equilibrium. It may be seen from Fig. 2 that the time taken by the neutral particles to flow through the region of the temperature maximum remains much shorter than the time required to traverse the entire shock width. In Fig. 3, the time-scale for collisional dissociation of H_2 is plotted as a function of the flow time for the model in which $v_{\text{s}} = 70 \text{ km s}^{-1}$. The dissociation time varies rapidly with T_{n} , owing to the exponential dependence of the dissociation rate coefficient (cf. Section 2.3). Thus, the dissociation time can become comparable with the flow time in the region of the maximum of T_{n} but increases rapidly as the gas cools. The time-scale for dissociation becomes too large for dissociation to be completed within the flow time,

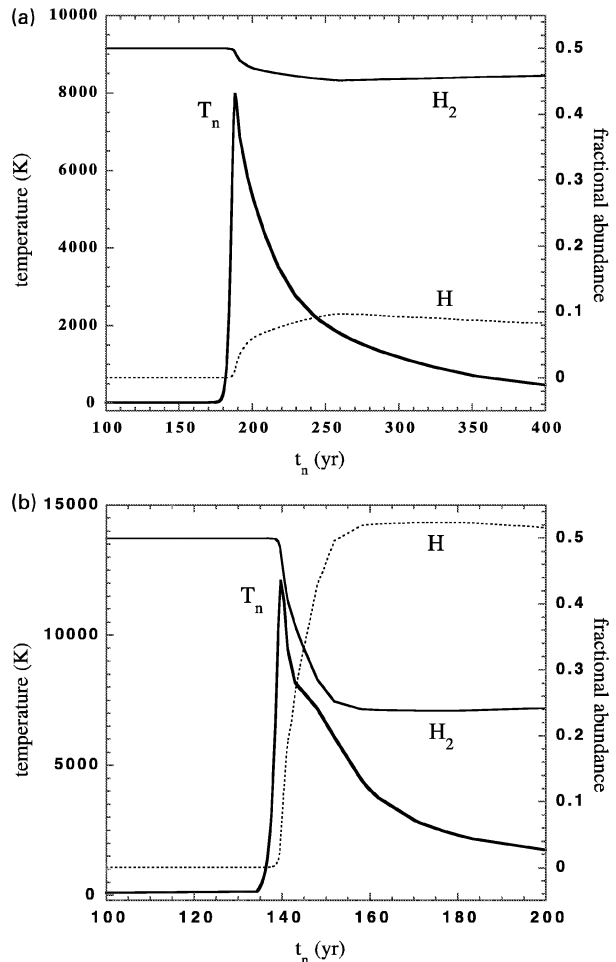


Figure 2. The profile of the temperature of the neutral fluid, T_{n} , and the abundances of atomic and molecular hydrogen, relative to $n_{\text{H}} = n(\text{H}) + 2n(\text{H}_2)$, for models in which, initially, $n_{\text{H}} = 10^4 \text{ cm}^{-3}$, $n(\text{ortho } \text{H}_2)/n(\text{para } \text{H}_2) = 3.0$, $n(\text{H})/n(\text{H}_2) = 7.4 \times 10^{-4}$ and (a) $v_{\text{s}} = 60 \text{ km s}^{-1}$, (b) $v_{\text{s}} = 70 \text{ km s}^{-1}$; t_{n} is the flow time of the neutral fluid. Note the difference in the scales of the abscissa.

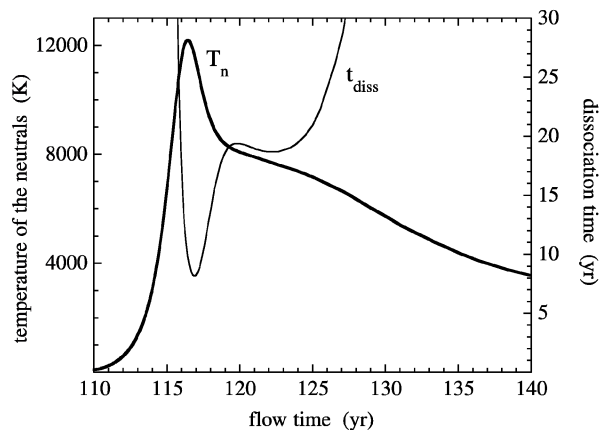


Figure 3. The time-scale for collisional dissociation of H_2 plotted as a function of the flow time of the neutral fluid for the model in Fig. 2(b), i.e. initially $n_{\text{H}} = 10^4 \text{ cm}^{-3}$, $n(\text{ortho } \text{H}_2)/n(\text{para } \text{H}_2) = 3.0$, $n(\text{H})/n(\text{H}_2) = 7.4 \times 10^{-4}$, and $v_{\text{s}} = 70 \text{ km s}^{-1}$.

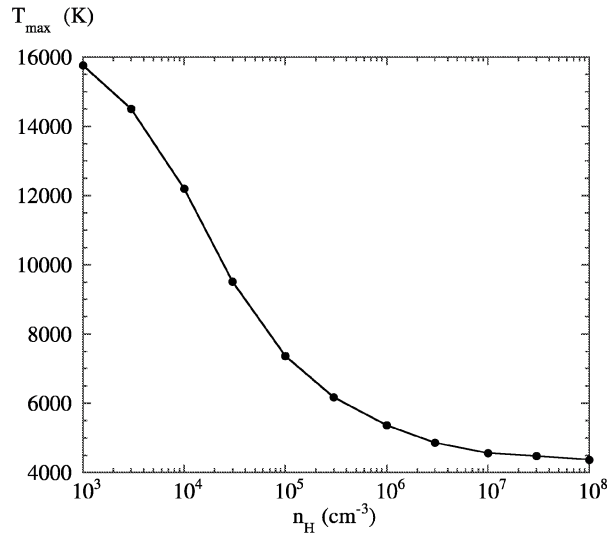


Figure 4. The maximum temperature attained by the neutral fluid, as a function of the pre-shock gas density, for shock velocities which are just subcritical. The initial value of the transverse magnetic induction is given by $B(\mu\text{G}) = [n_{\text{H}}(\text{cm}^{-3})]^{1/2}$.

even though a large fraction of the hydrogen is converted into atomic form, as is evident from Fig. 2(b). However, a small increase in v_s beyond its critical value is sufficient to precipitate a catastrophic rise in the kinetic temperature, associated with the dissociation of H_2 , which is the major coolant, and a sonic point is rapidly attained. The feedback loop involving the temperature and the rate of dissociation of H_2 is intrinsically non-linear, and the simultaneous solution of the equations specifying the relevant chemical and energetic effects and of the equations describing the fluid flow is essential to the reliable determination of v_{crit} .

In practice, we found that the dissociation of H_2 is initially dominated by non-thermal collisions with drifting ions but that thermal collisions with H_2 and H take over as the temperature of the neutrals rises; dissociation by electrons remains relatively unimportant throughout. However, ionization processes affect indirectly and significantly the rate of dissociation of H_2 and the value of the critical shock speed. The higher is the degree of ionization of the gas, the greater are the strength of ion-neutral coupling and hence the maximum kinetic temperature attained by the neutrals. The coupling of the neutral to the ionized fluid enhances the rate of decrease of v_n towards the adiabatic sound speed, which increases with the kinetic temperature. In Fig. 4, we plot the maximum temperature attained by the neutral fluid, as a function of the pre-shock gas density, for shock velocities which are just sub-critical, and for which a C-type solution exists. The curve in this figure represents the maximum temperature which can be reached in a C-type shock wave, assuming $B(\mu\text{G}) = [n_{\text{H}}(\text{cm}^{-3})]^{1/2}$ initially. The maximum temperature decreases with increasing density, but collisional dissociation of H_2 still takes place: because of the tendency towards thermalization of the energy levels at high density, dissociation occurs increasingly from excited molecular states, which have lower dissociation threshold energies. The rate of cooling of the gas by H_2 tends to vary linearly (rather than quadratically) with n_{H} at high densities, and hence the energy dissipated by the shock wave is less rapidly evacuated and a sonic point is more readily attained.

The variation of v_{crit} with the initial value of the magnetic induction, $B(\mu\text{G}) = b[n_{\text{H}}(\text{cm}^{-3})]^{1/2}$, at a density of

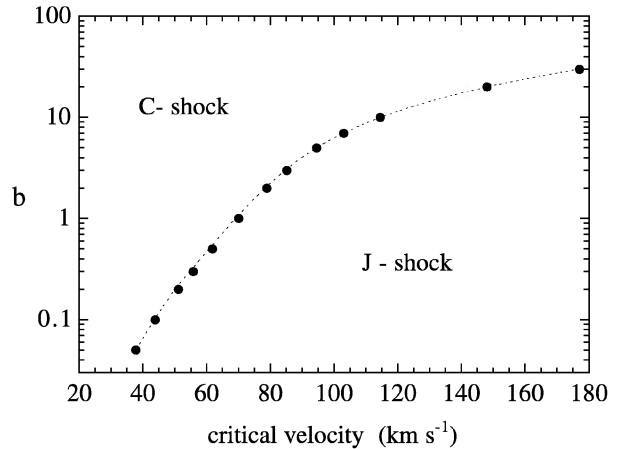


Figure 5. Maximum shock speed, v_{crit} , consistent with the existence of a C-type shock wave, as a function of the pre-shock magnetic induction, transverse to the flow, $B(\mu\text{G}) = b[n_{\text{H}}(\text{cm}^{-3})]^{1/2}$. The initial density is $n_{\text{H}} = 10^4 \text{ cm}^{-3}$ and the initial ortho:para H_2 ratio is 3.0.

$n_{\text{H}} = 10^4 \text{ cm}^{-3}$, is shown in Fig. 5. As B increases, the maximum temperature attained and hence the rate of collisional dissociation of H_2 decrease; but the time of flow through the (wider) shock wave increases, leaving sufficient time for dissociation to occur. Owing to the exponential dependence of the rate of dissociation on T_n , the net effect is an increase of v_{crit} with b ; v_{crit} is equal to 70 km s^{-1} for the reference value of $b = 1$.

3.2 Other molecular line cooling

Neufeld & Kaufman (1993) described an ‘escape probability’ approach to computing the rate of cooling of the interstellar medium owing to emission in lines of H_2O and CO . We have implemented their method and compared our results with the results obtained using a much simpler approximation, in which the cooling rates ($\text{erg cm}^{-3} \text{ s}^{-1}$) were calculated from the following expressions, appropriate to the limit of low densities:

$$\Gamma_{\text{H}_2\text{O}} = 1.0 \times 10^{-26} T_n \quad (2)$$

$$[n(\text{H}) + n(\text{H}_2)/2^{1/2}]n(\text{H}_2\text{O}) \exp(-35/T_n),$$

$$\Gamma_{\text{CO}} = 1.1 \times 10^{-28} T_n [n(\text{H}) + n(\text{H}_2)/2^{1/2}]n(\text{CO}) \exp(-5/T_n); \quad (3)$$

the factor of $2^{1/2}$ accounts for the larger mass (and lower collision frequency) of H_2 , relative to H . The fit, equation (2), to the rate of cooling by H_2O was derived by Flower (1989) on the assumption of low optical depths in the lines. The rate of CO cooling, equation (3), has the same functional form and is based on the assumption that only ^{13}CO cools significantly, as the lines of ^{12}CO become optically thick; the adopted $^{12}\text{CO}:^{13}\text{CO}$ abundance ratio is 90:1. The rates of cooling by OH and NH_3 were also taken into account, using expressions analogous to (2) but with 120 K (for OH) and 40 K (for NH_3) in the numerator of the argument of the exponential (cf. Flower & Pineau des Forêts 1994, section 2.3).

In Fig. 6, we compare the H_2O and CO cooling rates predicted using equations (2) and (3) with those calculated following Neufeld & Kaufman (1993), for a model in which $v_s = 60 \text{ km s}^{-1}$, and initially $n_{\text{H}} = 10^4 \text{ cm}^{-3}$, $B = 100 \mu\text{G}$, and $n(\text{ortho } \text{H}_2)/n(\text{para } \text{H}_2) = 3.0$. It may be seen that the rates of cooling by H_2O , computed by means of the escape probability method and by using equation (2), agree well in the hot gas, where

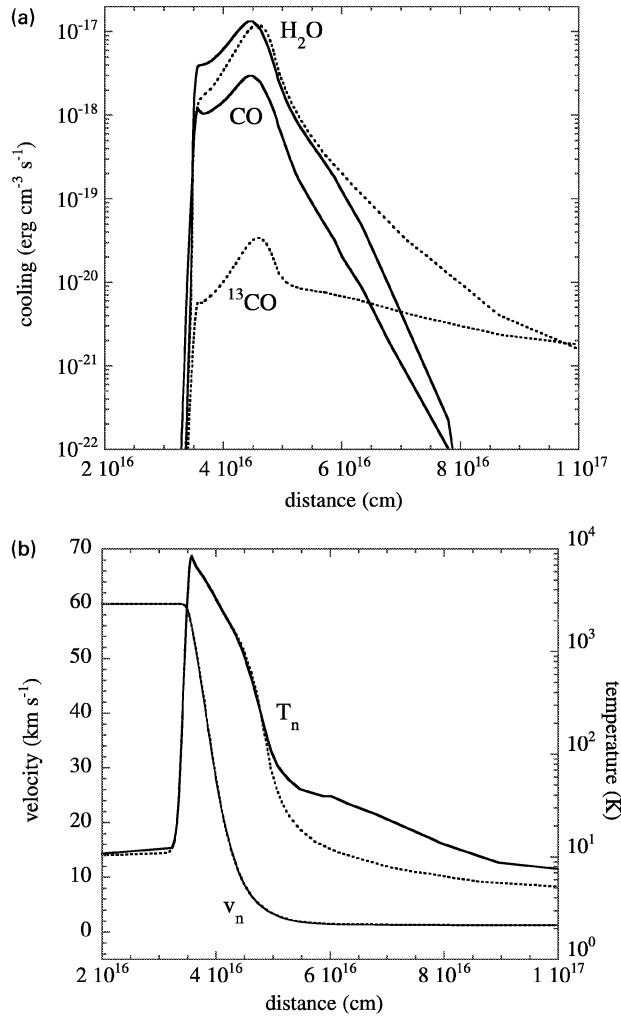


Figure 6. (a) Rates of cooling by H₂O and CO, computed following the ‘escape probability’ approach of Neufeld & Kaufman (1993) (full lines) or by means of equations (2) and (3), respectively (broken lines). The corresponding velocity and temperature profiles of the neutral fluid are plotted in (b).

the velocity gradient is large and optical depth effects are small. However, equation (3) underestimates the rate of cooling by CO in the hot gas and appears to overestimate this cooling rate as the temperature of the gas decreases towards its (post-shock) equilibrium value. The discrepancy in the hot gas arises because the ¹²CO lines are optically thin, owing to the large velocity gradient in this part of the shock wave. The escape probability method then yields a CO cooling rate which is larger than that derived from equation (3) by approximately the ¹²C:¹³C isotope ratio. In the post-shock gas, on the other hand, the lines of ¹²CO become optically thick and the associated cooling rate falls steeply. Cooling by ¹³CO might then predominate, as Fig. 6(a) suggests, but the implications for the column densities of the excited rovibrational levels of H₂ are minimal, as higher temperatures are required to populate these states.

3.3 Comparison with ISO observations of Orion

3.3.1 H₂ lines

Rosenthal, Bertoldi & Drapatz (2000) reported observations of the

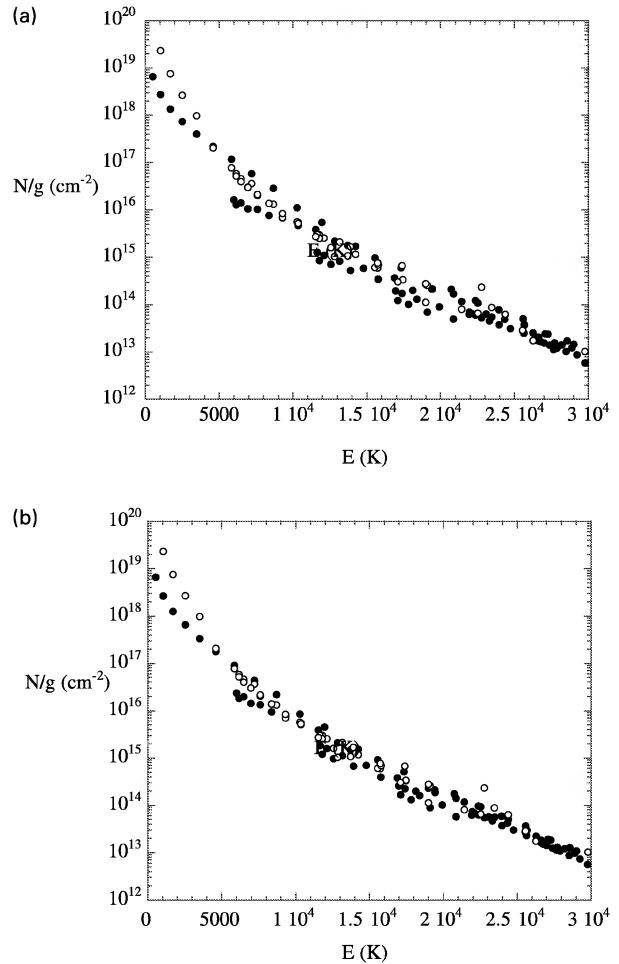


Figure 7. Excitation diagram for the H₂ lines observed in emission from Orion by ISO-SWS (Rosenthal et al. 2000: open circles). The column densities, $N_{v,J}$, of the rovibrational levels (v, J) are divided by their statistical weights, $g_{v,J} = (2J + 1)$ for J even or $3(2J + 1)$ for J odd, and plotted against their energies, $E_{v,J}$, relative to the $v = 0, J = 0$ ground state. Calculated points (filled circles) from a model in which $v_s = 60 \text{ km s}^{-1}$, $n_{\text{H}} = 10^4 \text{ cm}^{-3}$, $B = 100 \mu\text{G}$, $n(\text{ortho H}_2)/n(\text{para H}_2) = 3.0$, and, initially, (a) $n(\text{H})/n(\text{H}_2) = 7.4 \times 10^{-4}$, (b) $n(\text{H})/n(\text{H}_2) = 0.5$.

Orion Molecular Cloud Peak 1 (OMC-1) in emission lines of H₂, made with the short-wave spectrometer (SWS) on the *Infrared Space Observatory* (ISO). Lines were observed from rovibrational levels with a wide range of excitation energies, extending from $v = 0, J = 3$ ($E_{v,J} = 1015 \text{ K}$, relative to $v = 0, J = 0$) to a possible detection of $v = 0, J = 27$ ($E_{v,J} = 42515 \text{ K}$), and including levels with $0 \leq v \leq 4$. All but two of the lines which were detected are from levels with excitation energies $E_{v,J} < 30000 \text{ K}$; we consider first this energy range.

In Fig. 7, we compare the observations of Rosenthal et al. (2000) with the results of our model, using the initial values $v_s = 60 \text{ km s}^{-1}$, $n_{\text{H}} = 10^4 \text{ cm}^{-3}$, $B = 100 \mu\text{G}$, and $n(\text{ortho H}_2)/n(\text{para H}_2) = 3.0$. In Fig. 7(a), the ratio $n(\text{H})/n(\text{H}_2)$ has its pre-shock equilibrium value of 7.4×10^{-4} , whereas, in Fig. 7(b), this ratio is set initially equal to 0.5. The rate coefficients for vibrational excitation of H₂ by H are typically two orders of magnitude larger than for excitation by He or H₂ (see Le Bourlot et al. 1999). Consequently, the vibrational thresholds are less prominent in the theoretical results plotted in Fig. 7(b), in which the initial

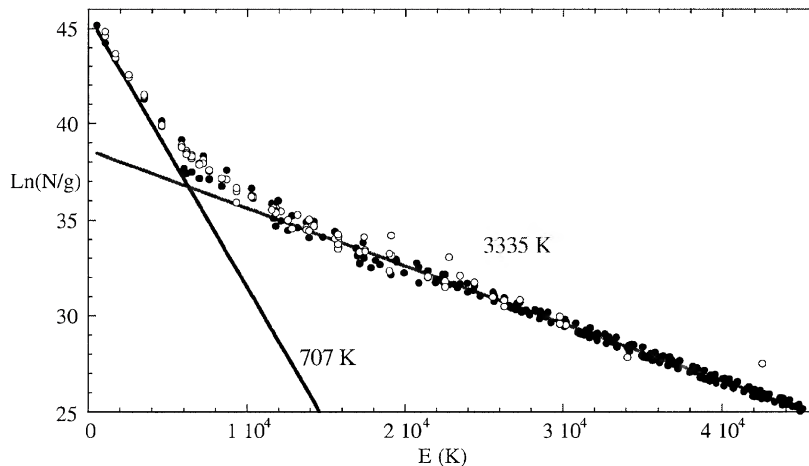


Figure 8. Excitation diagram, in the range of energies $E_{vJ} < 45\,000$ K. The model (filled circles) is that of Fig. 7(b), to which the contributions to the column densities from a lower excitation C-type shock ($v_s = 40\text{ km s}^{-1}$, $n_H = 10^4\text{ cm}^{-3}$, $B = 400\text{ }\mu\text{G}$, and $n(\text{ortho H}_2)/n(\text{para H}_2) = 3.0$) have been added. The open circles denote the observations of Rosenthal et al. (2000). The best-fitting excitation temperatures are also given.

abundance of H is comparable with those of He and H_2 , than in Fig. 7(a). In this respect, the results in Fig. 7(b) are in better agreement with the observations of Rosenthal et al. (2000). With the exception of the still incompletely thermalized $v = 1$ vibrational band, we consider that, from level $v = 0$, $J = 7$ ($E_{vJ} = 4587\text{ K}$) upwards, the calculations in Fig. 7(b) are in good agreement with the observations. For levels $v = 0$, $3 \leq J \leq 6$, the measured points are up to an order of magnitude (for $J = 3$) above the corresponding calculated points. The existence of high column densities of H_2 in the low levels of excitation suggests the presence, in the ISO-SWS field of view, of another shock wave in which the kinetic temperature attains a lower maximum value.

Pre-shock gas densities higher than the above value ($n_H = 10^4\text{ cm}^{-3}$) were indicated by previous studies of OMC-1 (Draine & Roberge 1982; Chernoff, Hollenbach & McKee 1982), and we also have computed models with higher initial densities (see below). However, we found that increasing the pre-shock density to $n_H = 10^5\text{ cm}^{-3}$, for example, leads to overestimating the column densities at intermediate levels of excitation ($5000 < E_{vJ} < 15\,000\text{ K}$), by factors of typically 5.

In Fig. 8, we plot the complete set of observations of Rosenthal et al. (2000), together with the sums of the values of $N_{vJ}g_{vJ}$ from the model in Fig. 7(b) [$v_s = 60\text{ km s}^{-1}$, $n_H = 10^4\text{ cm}^{-3}$, $B = 100\text{ }\mu\text{G}$, $n(\text{ortho H}_2)/n(\text{para H}_2) = 3.0$, $n(\text{H})/n(\text{H}_2) = 0.5$] and a lower excitation model in which $v_s = 40\text{ km s}^{-1}$, $n_H = 10^4\text{ cm}^{-3}$, $B = 400\text{ }\mu\text{G}$, $n(\text{ortho H}_2)/n(\text{para H}_2) = 3.0$, $n(\text{H})/n(\text{H}_2) = 7.4 \times 10^{-4}$ initially. The lower excitation model contributes exclusively to the populations of the levels $v = 0$, $J < 7$; the combination of a lower shock speed ($v_s = 40\text{ km s}^{-1}$) and a higher initial magnetic induction ($B = 400\text{ }\mu\text{G}$) suppresses the maximum kinetic temperature, from approximately 8000 K (cf. Fig. 2) to approximately 1450 K, and increases the width of the shock wave by more than an order of magnitude. The initial value of the ratio $n(\text{H})/n(\text{H}_2)$ is unimportant in this case, as vibrational excitation of H_2 is insignificant. We see from Fig. 8 that, apart from the deviation of the points just above the vibrational thresholds (particularly $v = 1$), the agreement with the observations is good. Nonetheless, we do not underestimate the possible significance of the sub-thermal excitation of $v = 1$ in the model. This discrepancy merits further investigation and will form part of a more comprehensive study of the OMC-1 region, which we plan to undertake in the near future.

Rosenthal et al. (2000) considered various physical processes which may give rise to the lines of H_2 . They concluded that the higher levels might be excited thermally in non-dissociative J-type shocks, non-thermally in C-type shocks (owing to the ion–neutral velocity difference), or during H_2 formation. Regarding the highest level which they detected, ($v = 0$, $J = 27$), they suggested that a process such as H_2 formation in the gas phase, in the reaction $\text{H}(\text{H}^-, \text{e}^-) \text{H}_2$, may have to be invoked to account for the observed column density.

It is apparent from Fig. 8 that the theoretical points pass between those representing the two highest energy levels that were observed. Both the observed and the calculated points scatter about a line the slope of which corresponds to an excitation temperature $T_{\text{exc}} = 3335\text{ K}$; this may be compared with the maximum temperature of almost 4500 K attained by the neutral fluid. Increasing the speed of the higher velocity component to, say, $v_s = 65\text{ km s}^{-1}$ enhances the excitation temperature and results in a theoretical curve which passes even closer to the column density of the highest energy level observed, ($v = 0$, $J = 27$). Our conclusion is that thermal excitation in a single C-type shock can probably account for the observations of the two highest energy levels. The evidence for non-thermal excitation of the 0–0 S(25) transition is not compelling, in the light of the present results. Rovibrational excitation of H_2 in collisions with charged grains (Pineau des Forêts et al. 2001) also proves to be of minor importance in the present context.

The predictions of planar C-type shock models with higher initial values of the gas density have been compared with the observations of H_2 in OMC-1. A model in which $n_H = 10^6\text{ cm}^{-3}$ and $v_s = 25\text{ km s}^{-1}$ yields good agreement with the observations of levels with $E_{vJ} \geq 20\,000\text{ K}$ but overestimates the column densities for $5000 \leq E_{vJ} \leq 20\,000\text{ K}$. Planar J-type shock waves have also been considered. In this case, agreement with the shape of the excitation diagram observed for $E_{vJ} \geq 6000\text{ K}$ is obtained when the pre-shock density $n_H = 10^6\text{ cm}^{-3}$ and $v_s = 10\text{ km s}^{-1}$. However, the absolute values of the column densities, integrated along the direction of propagation of the shock wave, are about 5 times smaller than observed. Additional assumptions – of several similar shock waves being present within the telescope beam, or of the shock wave being observed ‘edge-on’ – must then be made in order to bring the computed absolute values of the column densities

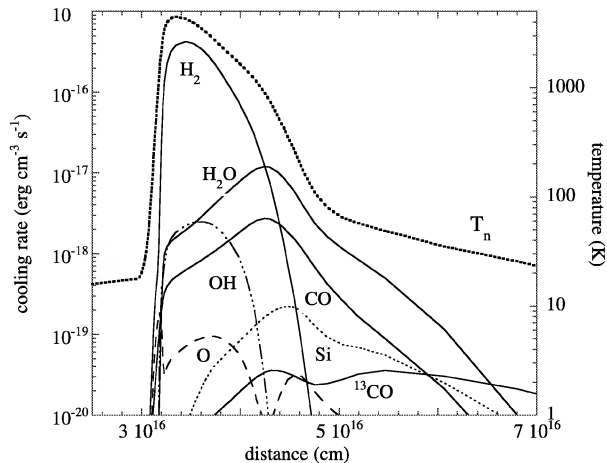


Figure 9. Contributions to the rate of cooling of the gas in the shock with $v_s = 60 \text{ km s}^{-1}$, $n_{\text{H}} = 10^4 \text{ cm}^{-3}$, $B = 100 \mu\text{G}$, $n(\text{ortho H}_2)/n(\text{para-H}_2) = 3.0$, $n(\text{H})/n(\text{H}_2) = 0.5$ initially.

into accord with those observed. Even so, the model underestimates, by factors which attain approximately 50 for $v = 0$, $J = 3$, the column densities of levels with $E_{vJ} \leq 6000 \text{ K}$. Thus, the key factors which enable the two-component model of planar C-type shock waves, presented above, to reproduce the observations of OMC-1 are:

(i) the high shock speeds which can be attained before the rapid onset of the dissociation of H_2 (cf. Section 3.1);

(ii) to a lesser degree, the assumption of an initial value of the ratio $n(\text{H})/n(\text{H}_2)$, which is higher than that in equilibrium in cold gas. Given the long time-scale for the reformation of H_2 (on grains), subsequent to its dissociation, a higher than equilibrium value of the H to H_2 density ratio could obtain in the region which has been perturbed by the OMC-1 outflow. The outflowing material is collimated and affects directly only a small fraction of the gas surrounding the protostar; but the gas which lies within the beam may have undergone compression and heating by an earlier shock wave. Species, such as H_2 , the reformation time-scale of which could exceed the time between the passage of successive shock waves, would then have abundances which differ from the values in chemical equilibrium.

3.3.2 Optically forbidden transitions of atoms and ions

In addition to the emission lines of H_2 , Rosenthal et al. (2000) observed optically forbidden transitions of atoms and ions, both in OMC-1 and in the Orion Bar photodissociation region (PDR). Lines from ions whose formation requires energies in excess of the H I Lyman limit (13.6 eV) arise from the region of ionized hydrogen ('H II' region). On the other hand, lines of [Si II], [S I] and [Fe II] might arise in shock-heated gas.

The intensity of the [Si II] 34.8- μm transition observed in OMC-1 was $1.5 \times 10^{-2} \text{ erg cm}^{-2} \text{ s}^{-1} \text{ sr}^{-1}$, whereas the intensity predicted by the higher velocity component, for which the principal cooling rates are plotted in Fig. 9, is of the order of $10^{-7} \text{ erg cm}^{-2} \text{ s}^{-1} \text{ sr}^{-1}$. We conclude that the shock wave(s) responsible for the H_2 emission do not contribute significantly to the intensity of the [Si II] line. The [Fe II] lines are observed to be one to two orders of magnitude less intense than the [Si II] line,

whilst [S I] 25.2 μm has comparable intensity ($1.2 \times 10^{-2} \text{ erg cm}^{-2} \text{ s}^{-1} \text{ sr}^{-1}$). Although the intensities of the [Fe II] and [S I] transitions are not currently calculated, we note that the fractional abundances of Fe^+ and S are between four and five orders of magnitude higher than that of Si^+ within the shock wave. It is conceivable, therefore, that the [Fe II] and [S I] transitions have their origin, at least partially, in the shock wave.

Gry et al. (1999) observed the Orion-KL nebula with the long wave spectrometer (LWS) on *ISO* and detected the $J = 2 \rightarrow 1$ fine structure transition of [Si I] at 68.5 μm , with an intensity of $(4.8 \pm 2) \times 10^{-5} \text{ erg cm}^{-2} \text{ s}^{-1} \text{ sr}^{-1}$ at a signal:noise ratio (S:N) of 5. Although Orion-KL is offset by about 25 arcsec from OMC-1, observed by Rosenthal et al. (2000), the *ISO*-LWS aperture was $81.5 \times 84.5 \text{ arcsec}^2$ at 68.5 μm , and so the field of view of Gry et al. (1999) would have included OMC Peak 1. The intensity that we calculate for the 68.5 μm transition is $10.7 \times 10^{-5} \text{ erg cm}^{-2} \text{ s}^{-1} \text{ sr}^{-1}$, about a factor of 2 higher than was observed. Given the low S:N ratio and the large aperture size, this level of agreement suggests that the [Si I] line may originate in OMC-1, rather than OMC-KL. On the other hand, the upper limit deduced by Gry et al. (1999) to the intensity of the $J = 1 \rightarrow 0$ transition at 129.7 μm ($1.1 \times 10^{-5} \text{ erg cm}^{-2} \text{ s}^{-1} \text{ sr}^{-1}$) is lower than the intensity that we calculate for this transition ($9.0 \times 10^{-5} \text{ erg cm}^{-2} \text{ s}^{-1} \text{ sr}^{-1}$).

Silicon is released from the refractory grain cores through sputtering by neutral particles impacting on the (charged) grains, at the ion-neutral drift speed; the fraction of Si released from the grains rises with the shock speed, as do the [Si I] line intensities. In our two-component model, the dominant contribution to the [Si I] lines arises from the shock wave with the higher speed of 60 km s^{-1} .

4 CONCLUDING REMARKS

We have summarized the characteristics of our C-type shock code MHD_VODE in Section 2 above. In Section 3, we specified the ranges of the shock parameters which define the grid of models that we are making available through <http://ccp7.dur.ac.uk>. We explained why the maximum permissible shock speed can exceed the values that had previously been believed to be upper limits.

We have compared the predictions of the model with *ISO*-SWS and *ISO*-LWS observations of OMC-1 and OMC-KL. A two-component model, comprising shocks with speeds of 60 km s^{-1} and 40 km s^{-1} , is found to yield good agreement with the observed column densities of rovibrational levels of H_2 extending up to $v = 0$, $J = 27$, which has an excitation energy of 42 515 K relative to the $v = 0$, $J = 0$ ground state. These shock speeds are higher and the pre-shock gas density ($n_{\text{H}} = 10^4 \text{ cm}^{-3}$) is lower than were derived by Draine & Roberge (1982) and Chernoff et al. (1982). We simply note that the *ISO* observations of H_2 rovibrational transitions (Rosenthal et al. 2000) and the rate coefficients pertaining to the collisional excitation of H_2 by the principal perturbers (Le Bourlot et al. 1999; Mandy & Martin 1993) represent vast improvements on the data available in 1982.

The high shock speeds attainable by the present models, before the rapid onset of the dissociation of H_2 , suggest that it may be possible to account not only for the column densities, but also for the profile of the 1-0 S(1) line observed in the Orion outflow (Brand et al. 1989), the width of which is of the order of 100 km s^{-1} . We plan to pursue this issue in a future study.

Draine & Roberge (1982) and Chernoff et al. (1982) also considered the emission by coolants other than H_2 , including CO, OH, H_2O and [O I]. In Table 1, we list the intensities in the lines of

Table 1. Calculated intensities ($\text{erg cm}^{-2} \text{s}^{-1} \text{sr}^{-1}$) in the lines of the species listed, which contribute to the cooling of the two component shock model of Fig. 8. The contributions of the two components are given separately, identified by the shock speed.

Coolant	60 km s^{-1}	40 km s^{-1}	Total
H ₂	0.1761	0.0242	0.2003
H ₂ O	0.00793	0.00693	0.0149
CO	0.00195	0.00244	0.00438
OH	0.00124	0.000005	0.00125
[O I]	0.000077	0.000208	0.000284
[Si I]	0.000197	0.000001	0.000198

these species, and also [Si I], which contribute to the cooling of the gas, and compare with H₂. For the $v_s = 60 \text{ km s}^{-1}$ component, we show in Fig. 9 the spatial distribution of the principal contributions to the cooling of the gas.

The dominance of the contribution of H₂ to the cooling of the shock-heated gas is evident from Table 1 and Fig. 9. Whilst the other species are minor coolants, their lines undoubtedly have diagnostic potential; more detailed analysis is deferred to a future study.

ACKNOWLEDGMENTS

One of the authors (DRF) gratefully acknowledges the award of a research fellowship by the Leverhulme Trust. We are indebted to David Wilgenbus for his contributions to updating the FORTRAN code.

REFERENCES

Anders E., Grevesse N., 1989, *Geochim. Cosmochim. Acta*, 53, 197
 Brand P. W. J. L., Toner M. P., Geballe T. R., Webster A. S., 1989, *MNRAS*, 237, 1009

Brown P. N., Byrne G. D., Hindmarsh A. C., 1989, *SIAM J. Sci. Stat. Comp.*, 10, 1038
 Chernoff D. F., Hollenbach D. J., McKee C. F., 1982, *ApJ*, 259, L97
 Dabrowski I., 1984, *Can. J. Phys.*, 62, 1639
 Dove J. E., Mandy M. E., 1986, *ApJ*, 311, L93
 Draine B. T., Roberge W. G., 1982, *ApJ*, 259, L91
 Draine B. T., Roberge W. G., Dalgarno A., 1983, *ApJ*, 264, 485
 Federman S. R., Shipsey E. J., 1983, *ApJ*, 269, 791
 Fite W. L., Brackmann R. T., 1958, *Phys. Rev.*, 112, 1141
 Flower D. R., 1989, *J. Phys. B*, 22, 2319
 Flower D. R., Pineau des Forêts G., 1994, *MNRAS*, 268, 724
 Flower D. R., Pineau des Forêts G., Field D., May P. W., 1996, *MNRAS*, 280, 447
 Gry C., Pineau des Forêts G., Walmsley C. M., 1999, *A&A*, 348, 227
 Heck L., Flower D. R., Pineau des Forêts G., 1990, *Computer Phys. Comm.*, 58, 169
 Hummer D. G., 1963, *MNRAS*, 125, 461
 Jacobs T. A., Giedt R. R., Cohen N., 1967, *J. Chem. Phys.*, 47, 54
 Kaufman M. J., Neufeld D. A., 1996a, *ApJ*, 456, 250
 Kaufman M. J., Neufeld D. A., 1996b, *ApJ*, 456, 611
 Le Bourlot J., Pineau des Forêts G., Roueff E., Flower D. R., 1993, *A&A*, 267, 233
 Le Bourlot J., Pineau des Forêts G., Flower D. R., 1999, *MNRAS*, 305, 802
 Mandy M. E., Martin P. G., 1993, *ApJS*, 86, 199
 May P. W., Pineau des Forêts G., Flower D. R., Field D., Allan N. L., Purton J. A., 2000, *MNRAS*, 318, 809
 Mendoza C., 1983, in Flower D. R., ed., *IAU Symp. 103, Planetary Nebulae*. Reidel, Dordrecht, p. 143
 Neufeld D. A., Kaufman M. J., 1993, *ApJ*, 418, 263
 Neufeld D. A., Melnick G. J., Harwit M., 1998, *ApJ*, 506, L75
 Pineau des Forêts G., Flower D. R., Dalgarno A., 1988, *MNRAS*, 235, 621
 Pineau des Forêts G., Flower D. R., Aguillon F., Sidis V., Sizun M., 2001, *MNRAS*, 323, L7
 Rapp D., Englander-Golden P., 1965, *J. Chem. Phys.*, 43, 1464
 Rosenthal D., Bertoldi F., Drapatz S., 2000, *A&A*, 356, 705
 Roueff E., 1990, *A&A*, 234, 567
 Shah M. B., Elliott D. S., Gilbody H. B., 1987, *J. Phys. B*, 20, 3501
 Smith M. D., Brand P. W. J. L., 1990, *MNRAS*, 242, 495
 Timmermann R., 1998, *ApJ*, 498, 246
 Wilgenbus D., Cabrit S., Pineau des Forêts G., Flower D. R., 2000, *A&A*, 356, 1010